Observational aspects of magnetic reconnection and energy release in solar flares:
The RHESSI perspective

Bhuwan Joshi
Udaipur Solar Observatory, Physical Research Laboratory, Udaipur, India

Collaborators: Astrid Veronig, Upendra Kushwaha, Yong-Jae Moon,
Kyung-Suk Cho, P. K. Manoharan, B. V. Somov

OUTLINE OF TALK

- Solar Flare
  - Classification, key components
- Temporal and spatial evolution
  - Multi-wavelength aspects of energy release
  - Development of a standard flare model
- New RHESSI observations
- Beyond "standard" flare
- Summary

Solar Flares

❖**Flares:** Transient, explosive perturbations in the solar atmosphere. (in excess of 10^{32} erg)

❖ Two broad categories: **Confined** and **Eruptive**

❖ **Magnetic reconnection** has been recognized as the the fundamental process for the rapid conversion of stored magnetic energy into heat and kinetic energy of plasma and particles.

❖ **Particle acceleration:** Electrons and ions accelerated to high energies escape into the interplanetary space or remain trapped in the corona and chromosphere.

❖ The properties of the **accelerated particles** are inferred from their radiative signature, as they interact with the solar plasma and magnetic fields.

❖ **Thermal & non-thermal emissions:** Plasma of wide range of temperatures (cool plasma eruption observed in Hα to a rapidly heated plasma in excess of 10 million K as recorded in X-rays); non-thermal particle (diagnosed in hard X-ray and radio): Multi-wavelength measurements are essential.

Near-limb X2.7/2B flare on 2003 November 3

Joshi et al. 2007, Solar Physics, 242, 143

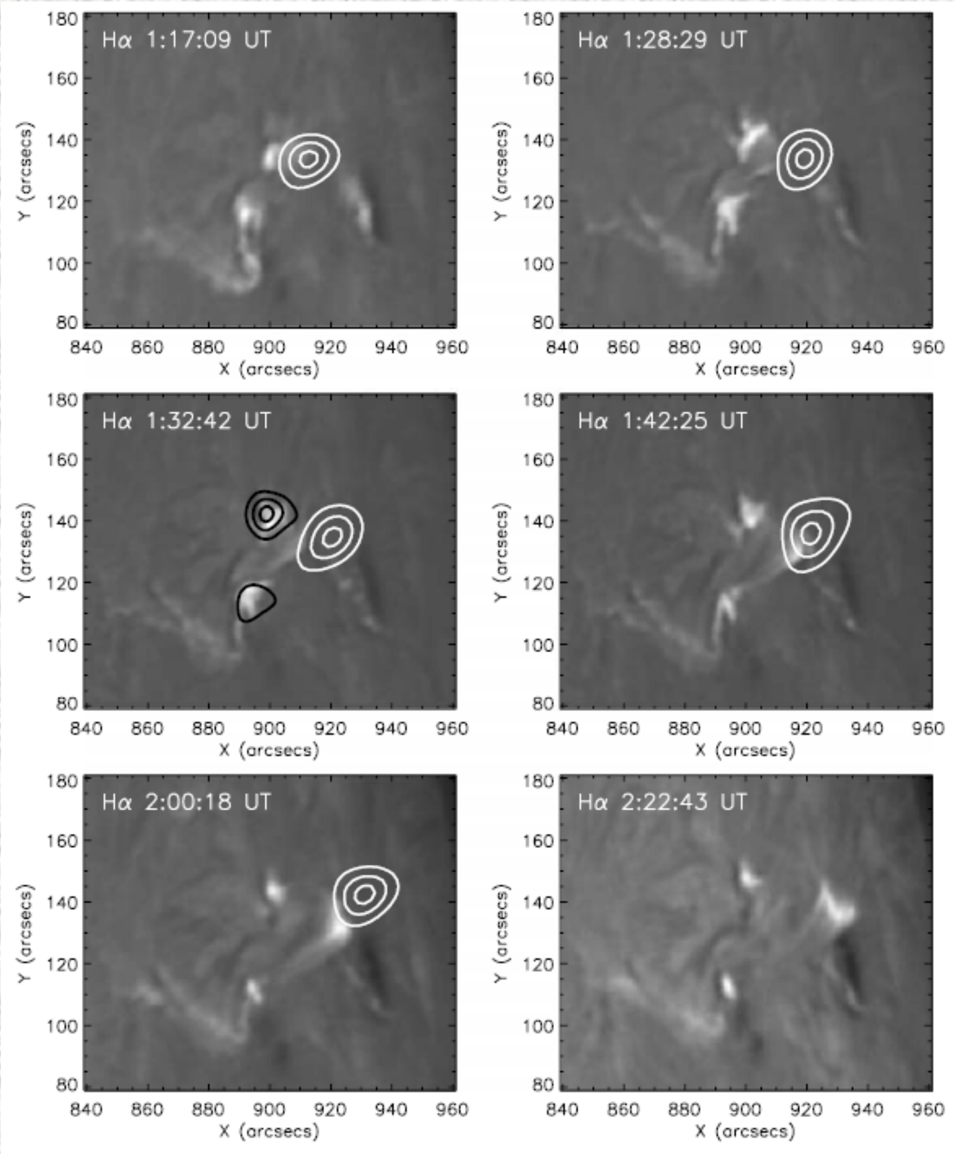

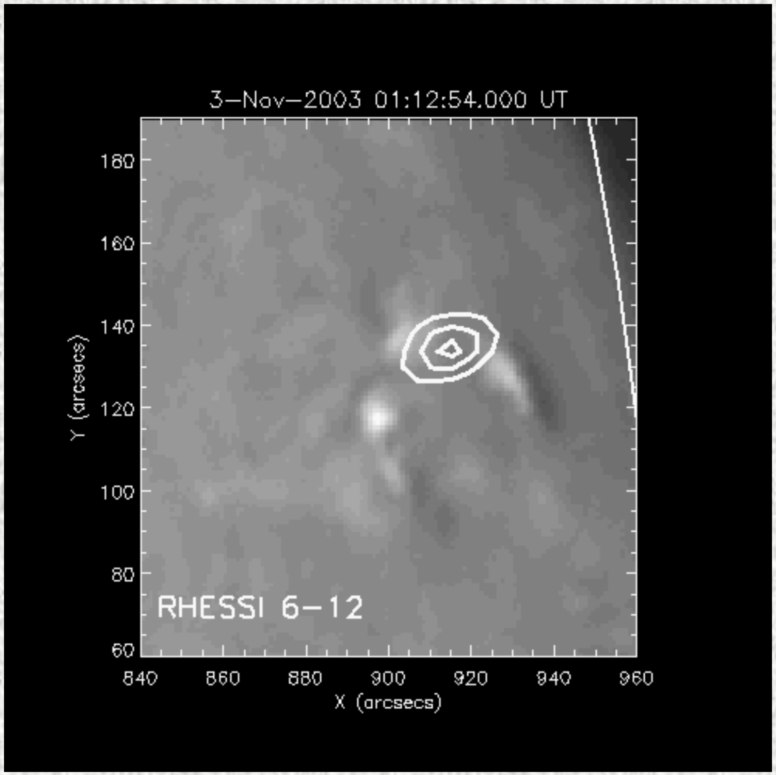

Hα data (ARIES solar telescope), India
RHESSI images: 6-12 keV (white contours)
50-100 keV (black contours)

Key components of a multi-wavelength flare

- ❑ Sigmoids

- ❑ Impulsive phase
  - Coronal emission, looptop sources
  - Footpoint sources, flare ribbons
  - Soft-hard-soft spectral evolution

- ❑ Gradual phase
  - Prolonged emission from hot coronal loops
  - Chormospheric evaporation
  - Neupert effect

- ❑ Cusp
  - Formation of cusp above the hottest outer loops

- ❑ Post-flare arcades

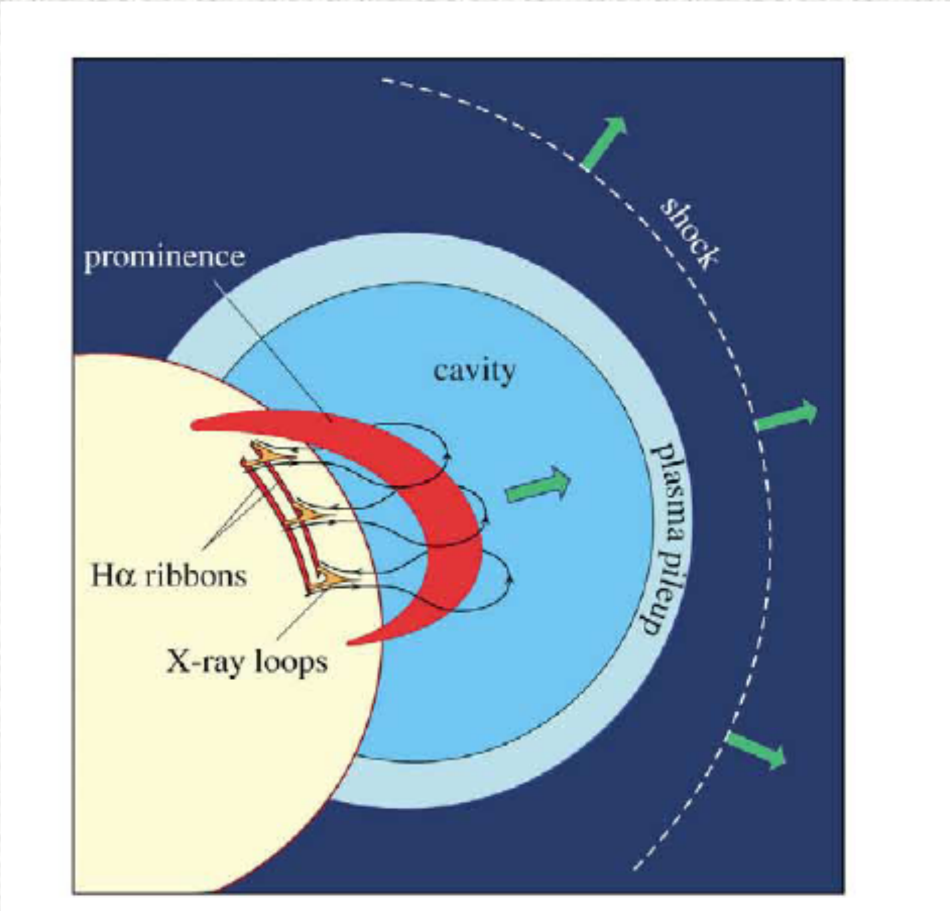

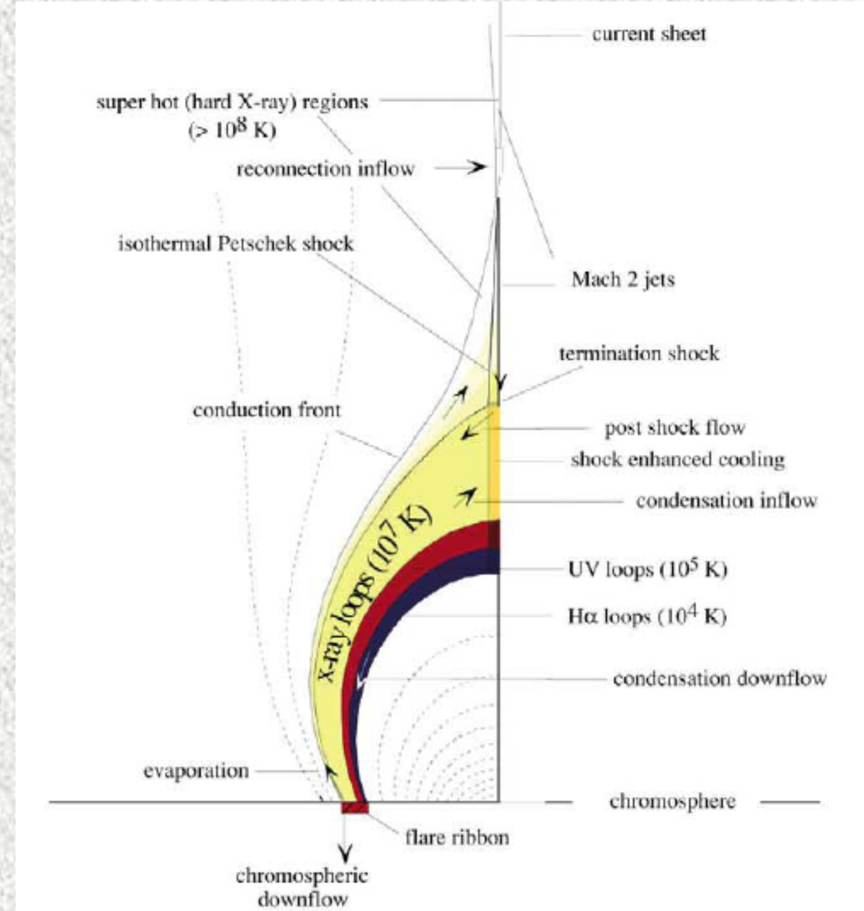

Schematic diagram of a two–ribbon flare and flare loop system.

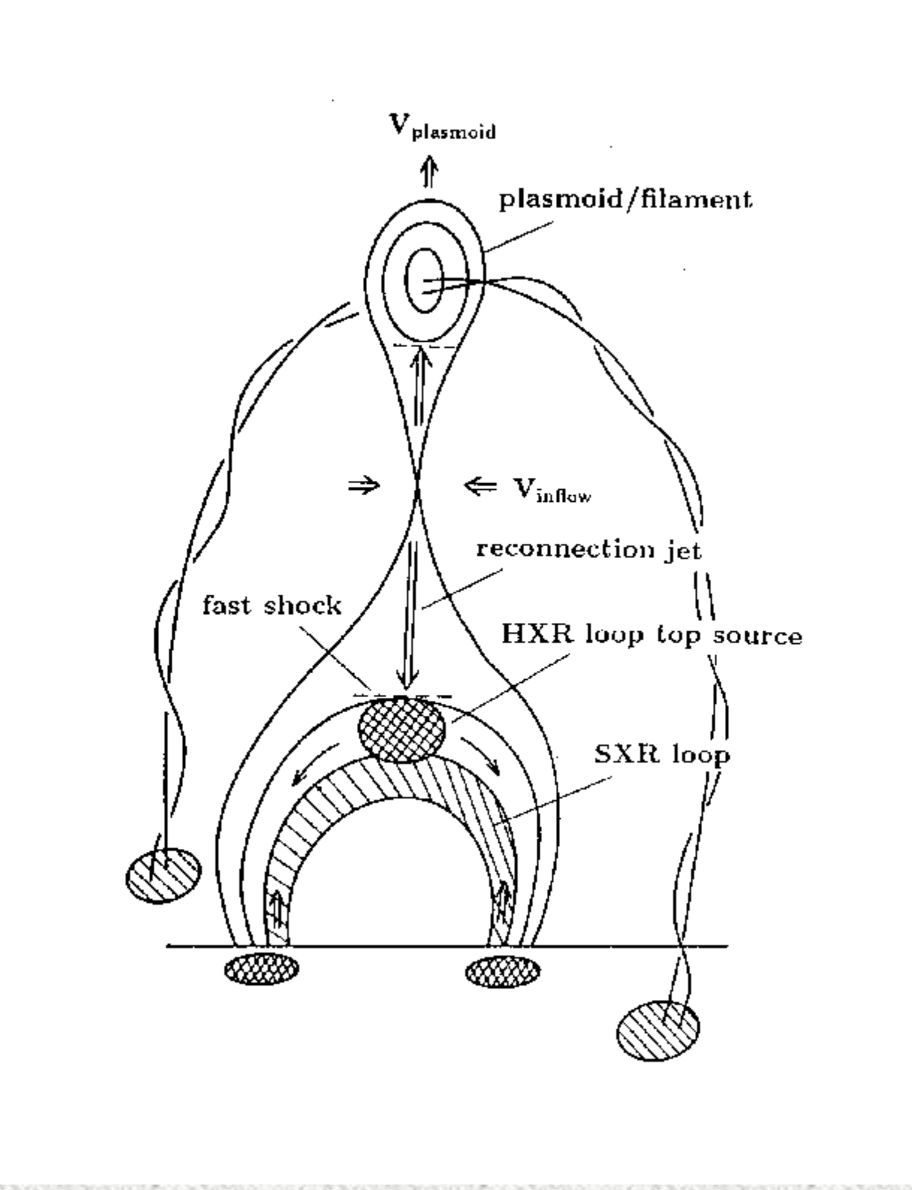

Plasmoid driven reconnection model (Shibata et al. 1998)

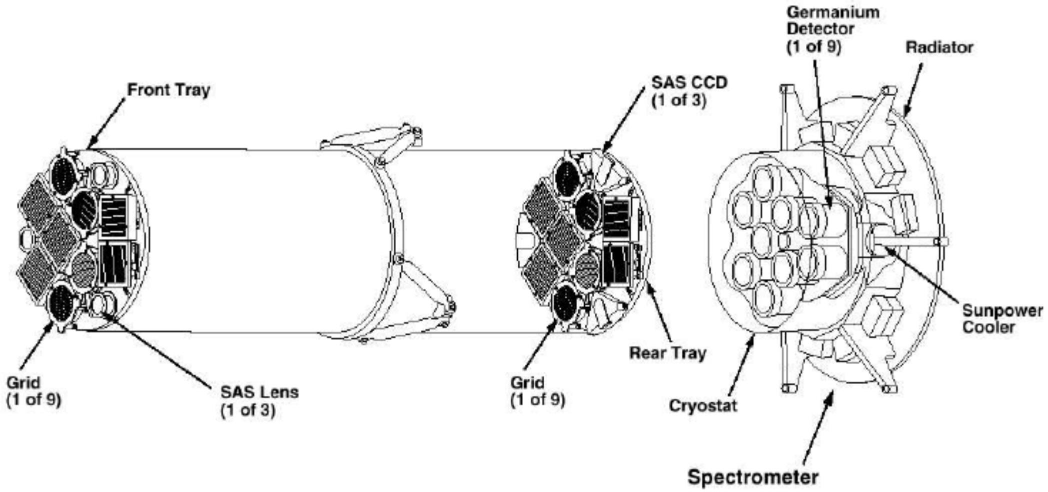

Figure 13.3: Layout of the RHESSI telescope that was mounted on a rotating spacecraft. The telescope (left) contains a set of nine front grids and nine identical rear grids which together modulate the incoming hard X-ray photons. The mounting of the nine grids (left) is also shown: The grid pitch (slit and slat) increases by a factor of $\sqrt{3}$ from grid 1 to 9, so that each one modulates a particular angular Fourier period. The modulated throughput is detected by nine cooled germanium detectors, one behind each of the rear grids (right), (Hurford et al. 2002).

Reuven Ramaty High Energy Solar Spectroscopic Images (RHESSI)

launched on February 5, 2002

New class of coronal HXR source at early rise phase

Lin et al. 2003, Asai et al. 2006, Veronig et al. 2006, Joshi et al. 2007

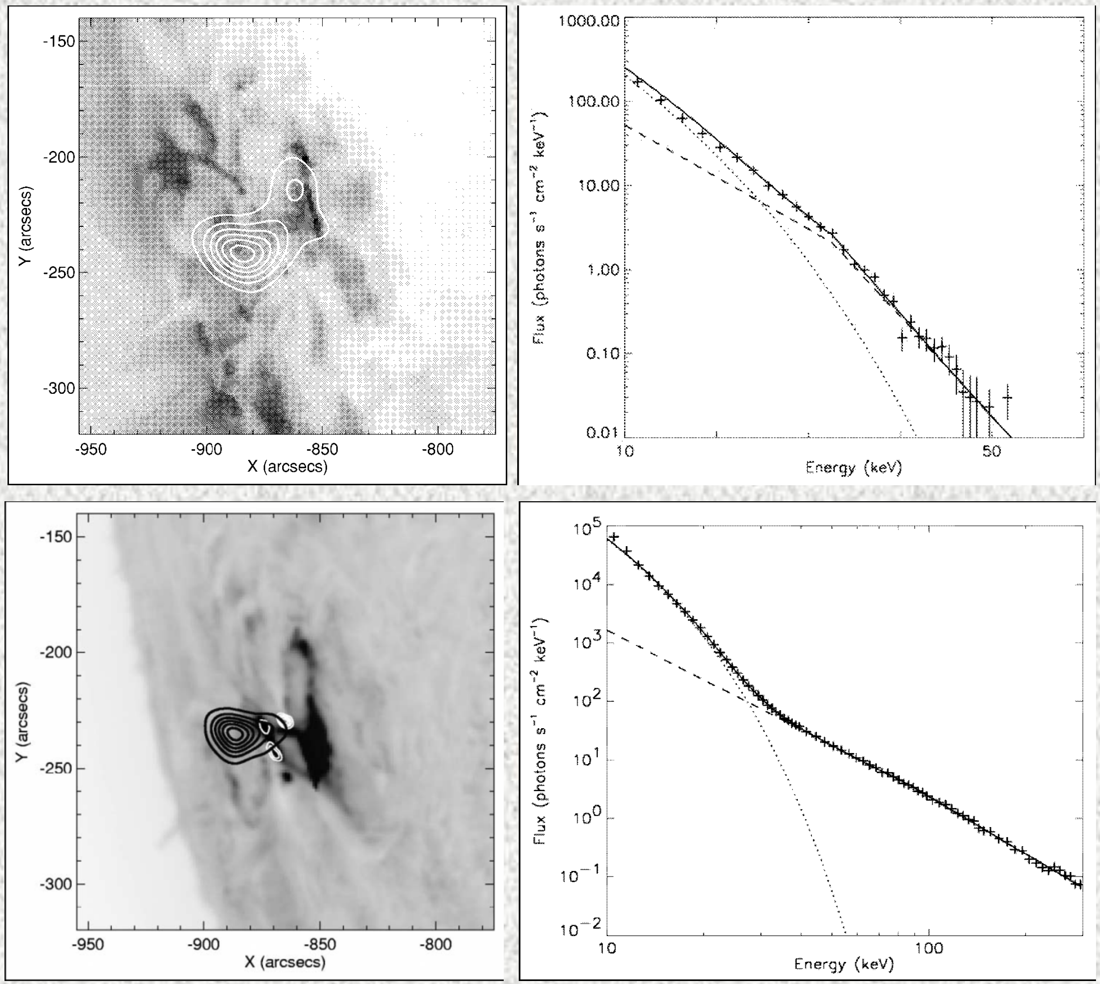

Coronal HXR sources in X4.8 flare on July 23, 2002 (Lin et al. 2003)

Top left: White contours (12-30 keV). Bottom left: Black contours:12-18 keV; white contours: 30-80 keV

Altitude decrease of LT source

Krucket et al. 2003, Sui & Holman 2003, Veronig et al. 2006, Joshi et al. 2007

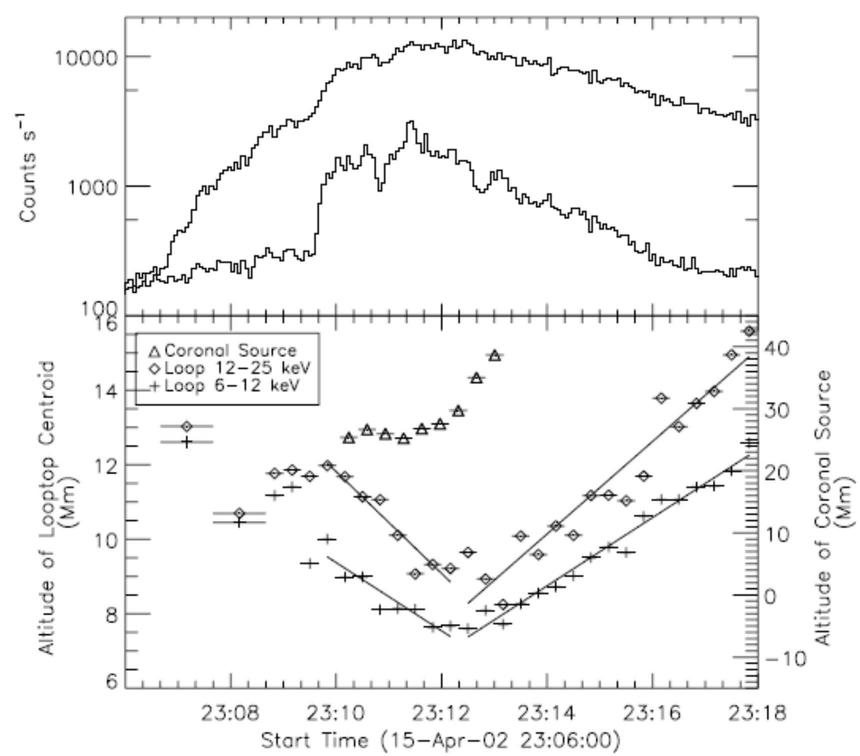

FIG. 6.—*Top*: Light curves in two energy bands (*upper curve*, 6–12 keV rate × 0.5; *lower curve*, 25–50 keV rate × 1.0) of the 2002 April 15 flare. *Bottom*: Altitude of the loop-top centroid obtained using the 60% contour for the images in the 6–12 (crosses) and 12–25 keV (*diamonds*) bands. The triangles show the altitude of the coronal source above the flare loop. The horizontal bars on each point represents the integration time of the corresponding image. The lines show linear fits to the altitudes vs. time for two time ranges and two energy bands.

SOL2002-04-15
M1.2 flare
(Sui et al. 2004)

X2.7 near limb flare SOL2003-11-03

Joshi et. al. 2007, Solar Physics

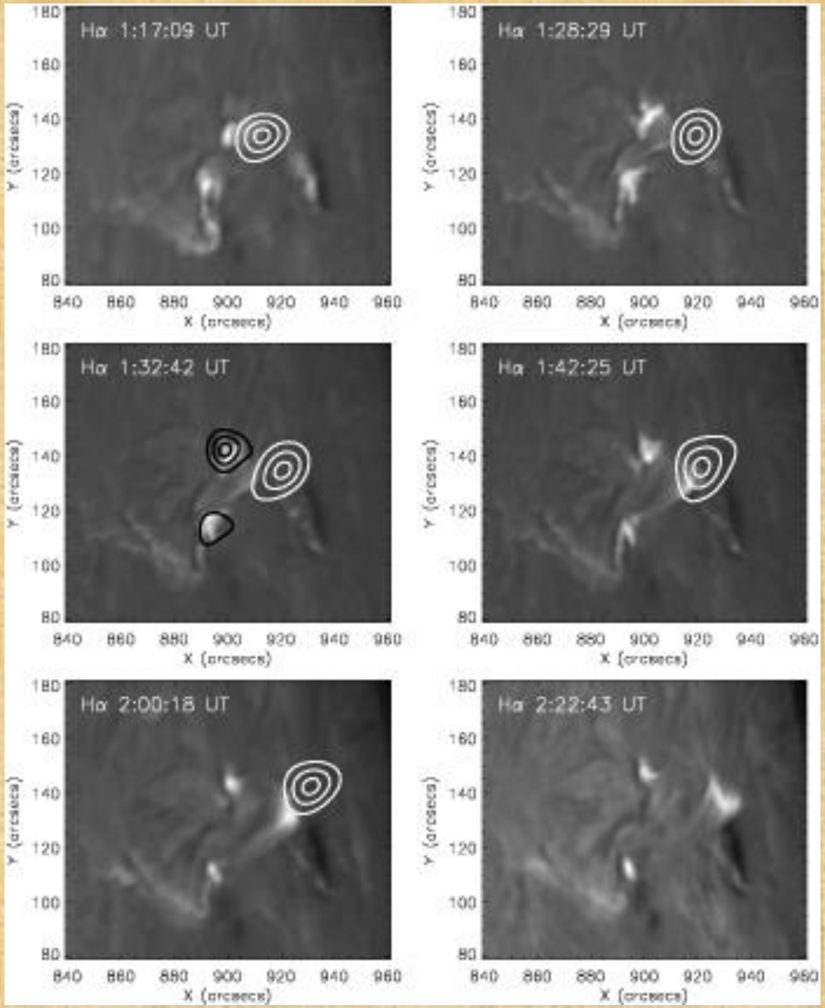

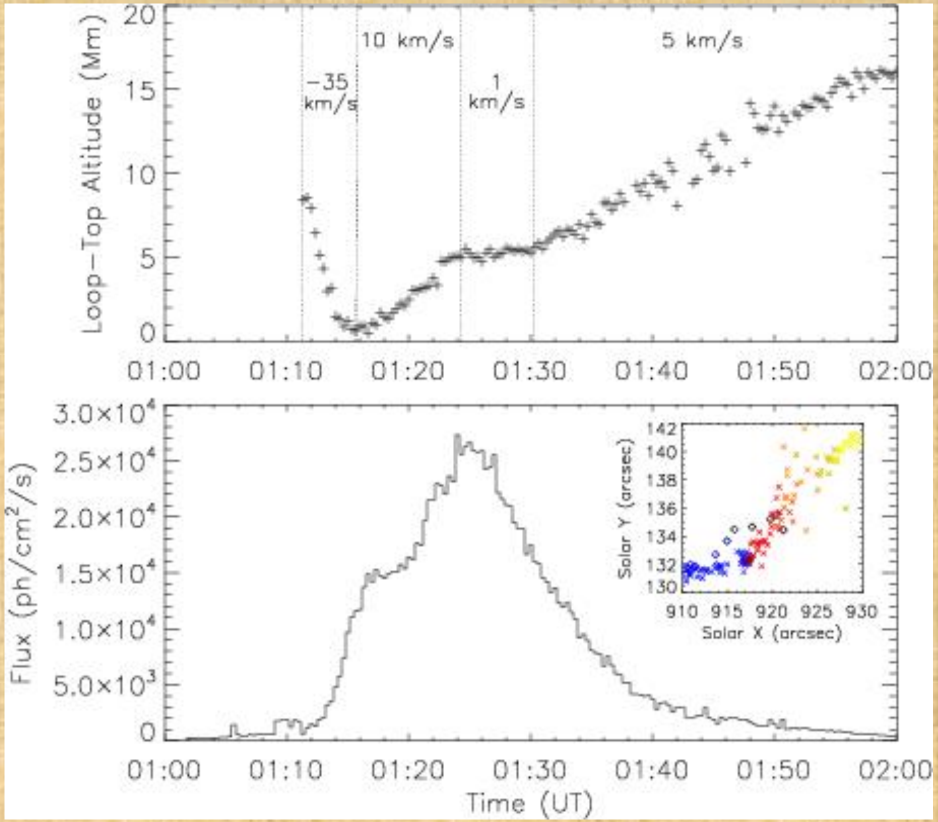

Sequence of Hα images overlayed by RHESSI
White contours: 10-15 keV, Black contours: 50-100 keV

Evidence for the formation of a large scale current sheet (HXR looptop and coronal source)

SOL2002 -04-15 (M1.2)

(Sui & Holman 2003; Sui et al. 2005)

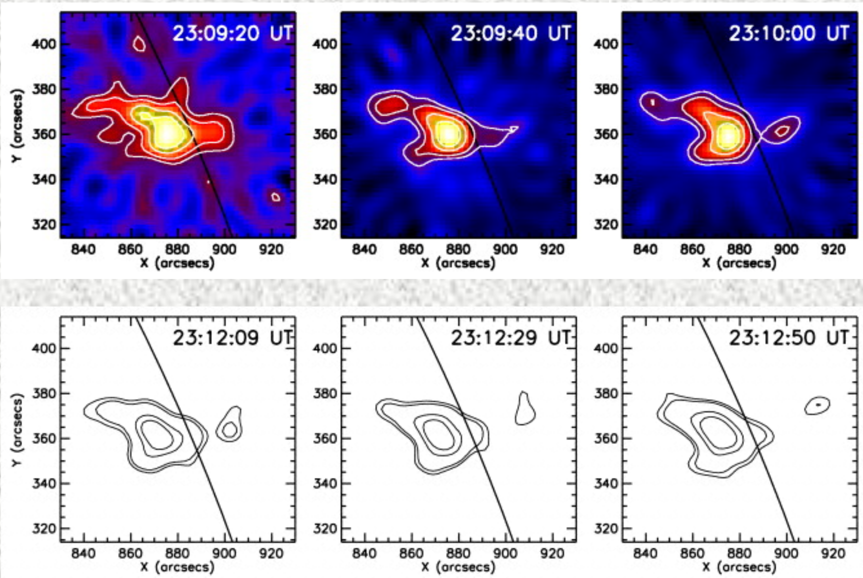

10-25 keV images of flare event on April 15, 2003

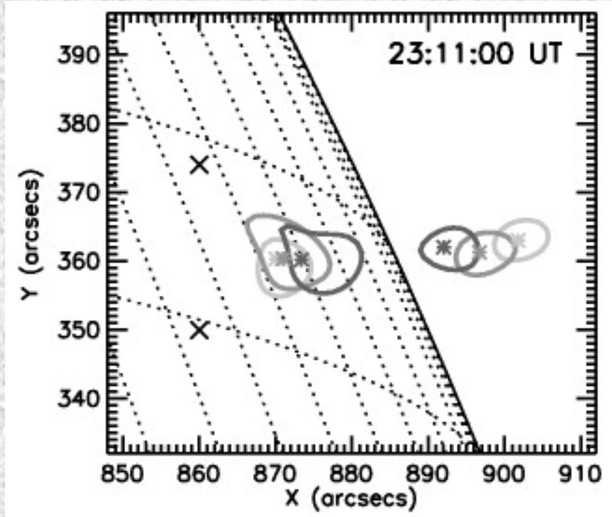

Solar disk: 6-8, 10-12, 16-20 keV (from light to dark)
Above the limb: 10-12, 12-14, 14-16 (from light to dark)
❑ *Temperature distribution indicates that a current sheet is formed between top of the flare loops and coronal source.*

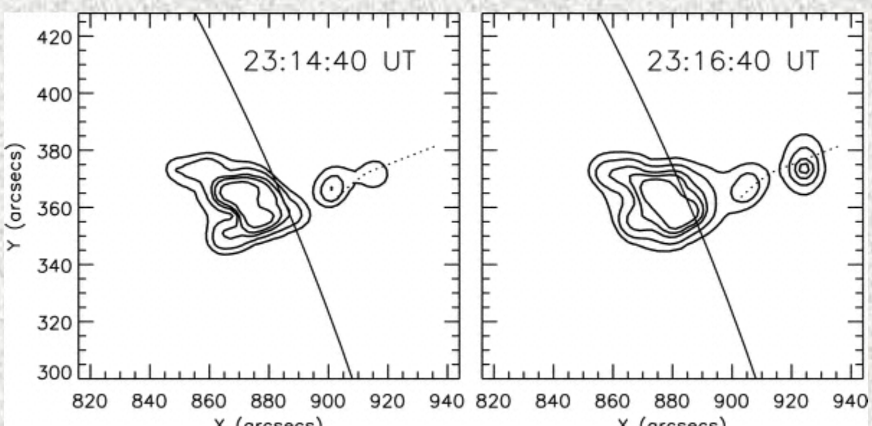

❖ **Coronal source speed > loop expansion speed Continuous elongation of current sheet (consistent with flare models, Priest & Forbes 2002)**

❖ **Appearances of blob-like sources along the trajectory of the initial coronal source above the loop: evidence for the growth of an instability within the current sheet.**

❖ **Tearing mode instability: As sheet lengthens, it is expected to occur and can produce distinct magnetic blobs with enhanced local heating of plasma.**

Double coronal hard and soft X-ray sources

Partially occulted M1.4 SOL 2002-04-30

(Liu, Petrosian, Dennis, & Jiang 2008)

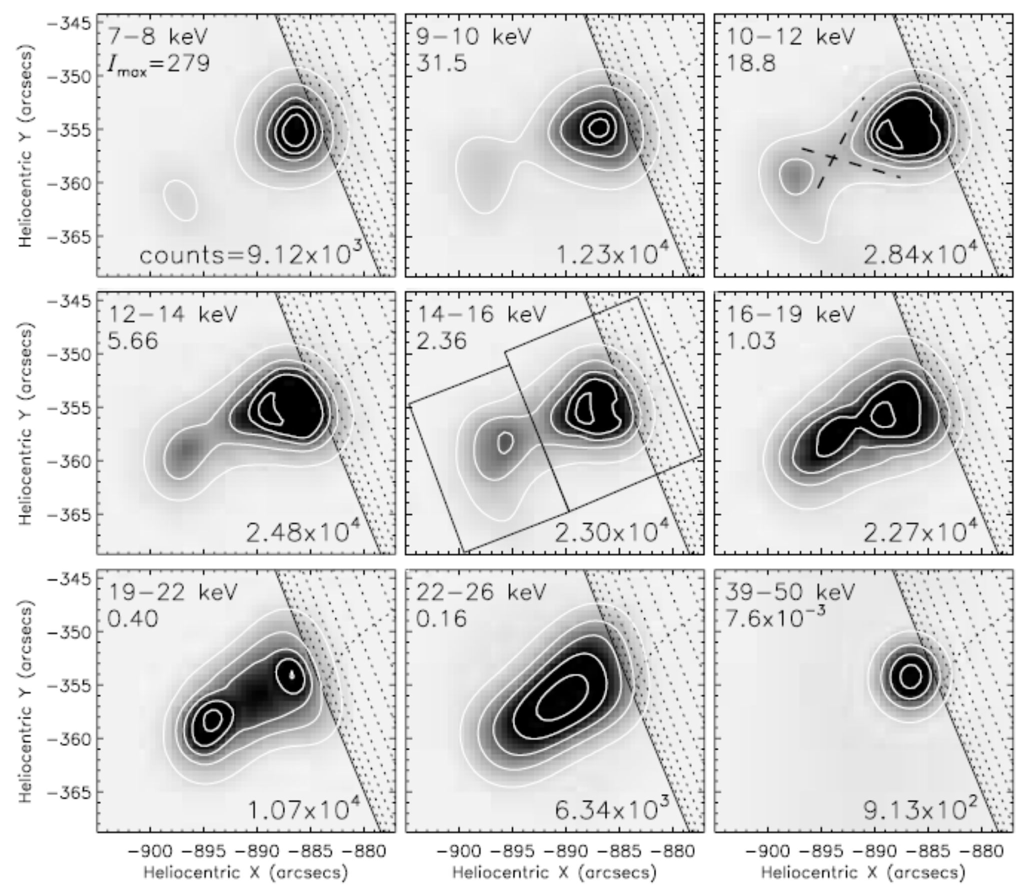

RHESSI images in different energy bands at 08:20:07-08:20:56 UT around maximum of main HXR peak.

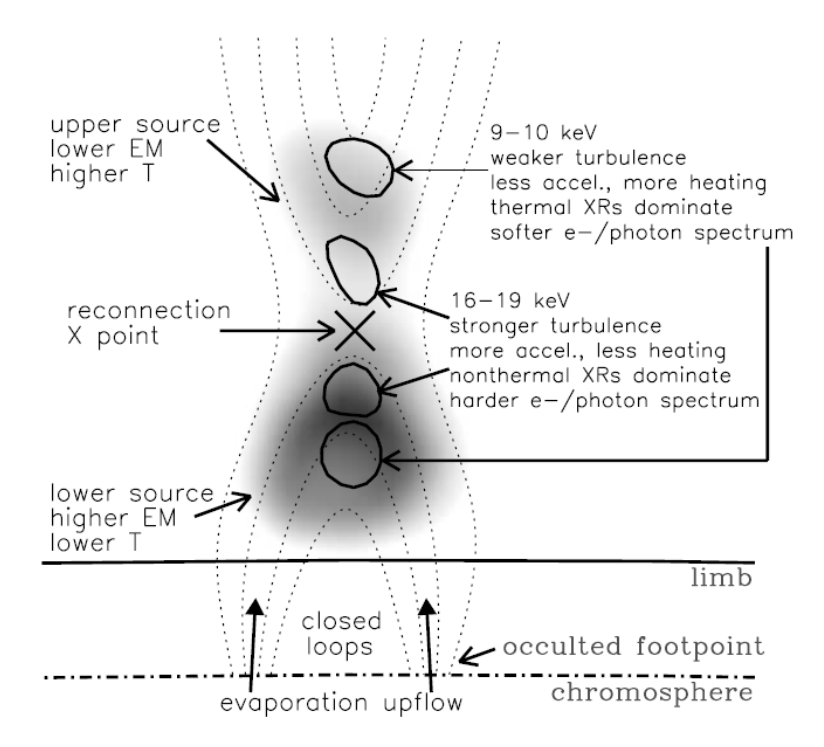

- ❑ Two coronal sources are observed for 12 minutes.
- ❑ Coronal sources exhibit energy dependent morphology: Higher energy emission originates from inner regions and energetically dominated by non-thermal emission.

Large-scale contractions of coronal loops SOL2003-10-24 (M7.6)

(Joshi et al. 2009, ApJ, 706,1438)

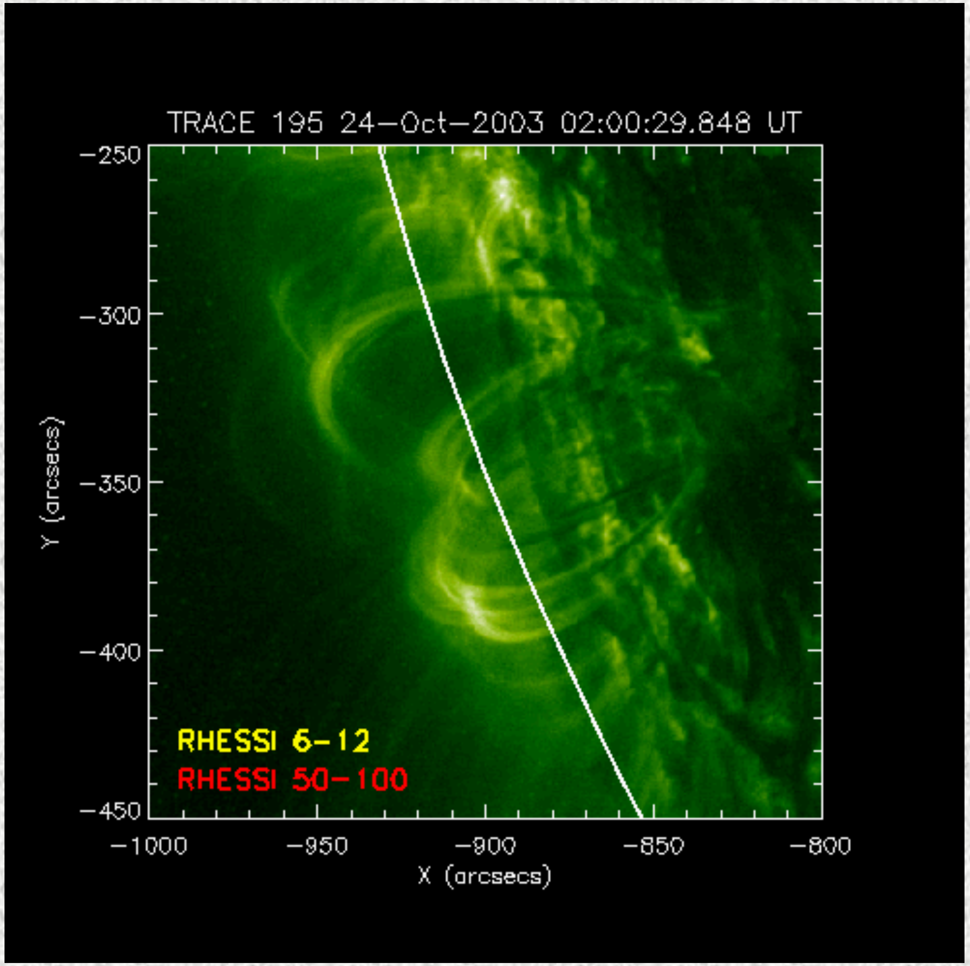

Two-phase evolution in terms of X-ray flux and flare morphology:
First phase (pre-heating phase): 02:24 – 02:44 UT; Second phase: from 02:44 onwards.

Large-scale contractions of coronal loops

(Joshi et al. 2009, ApJ, 706,1438)

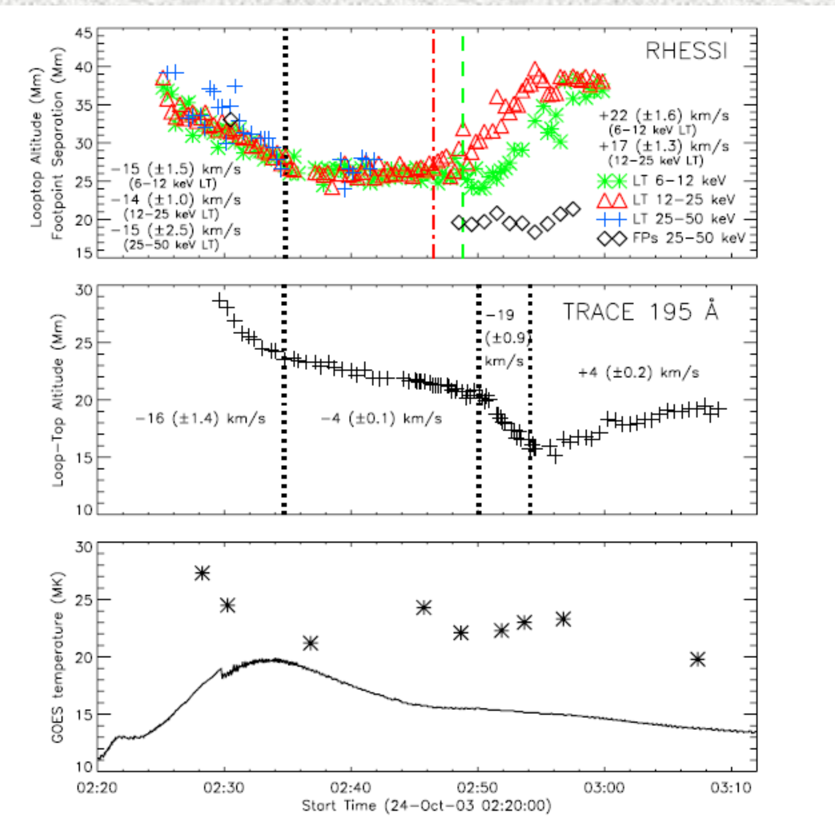

Phase I

- ❑ Descending X-ray LT source was observed for 11 minutes
- ❑ LT sources in different energy bands are almost co-spatial during the descending phase.

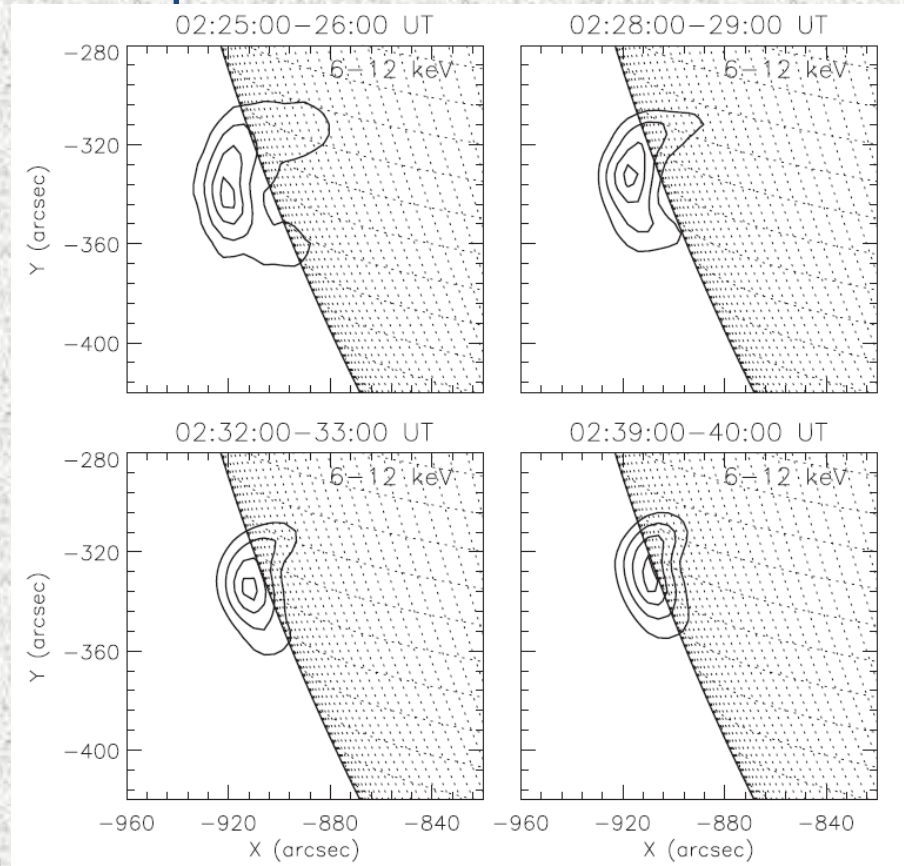

Phase II

- ❑ Emission at high energies originate at higher altitude during phase 2.

Large-scale contraction of coronal loops SOL2004-07-14 (M6.2)

(Kushwaha, Joshi, et al. 2015, ApJ, 807, 101)

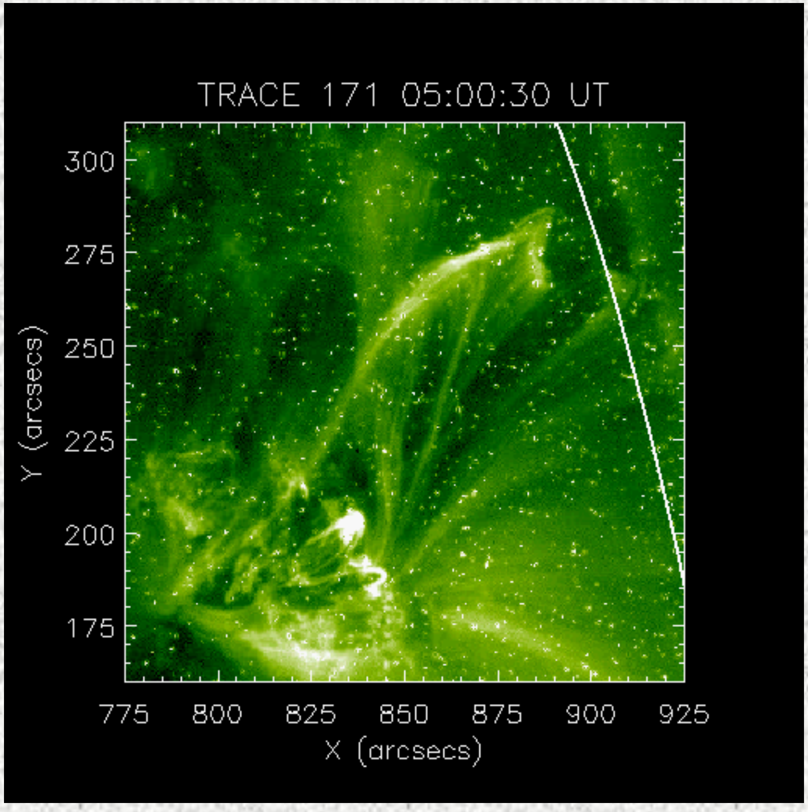

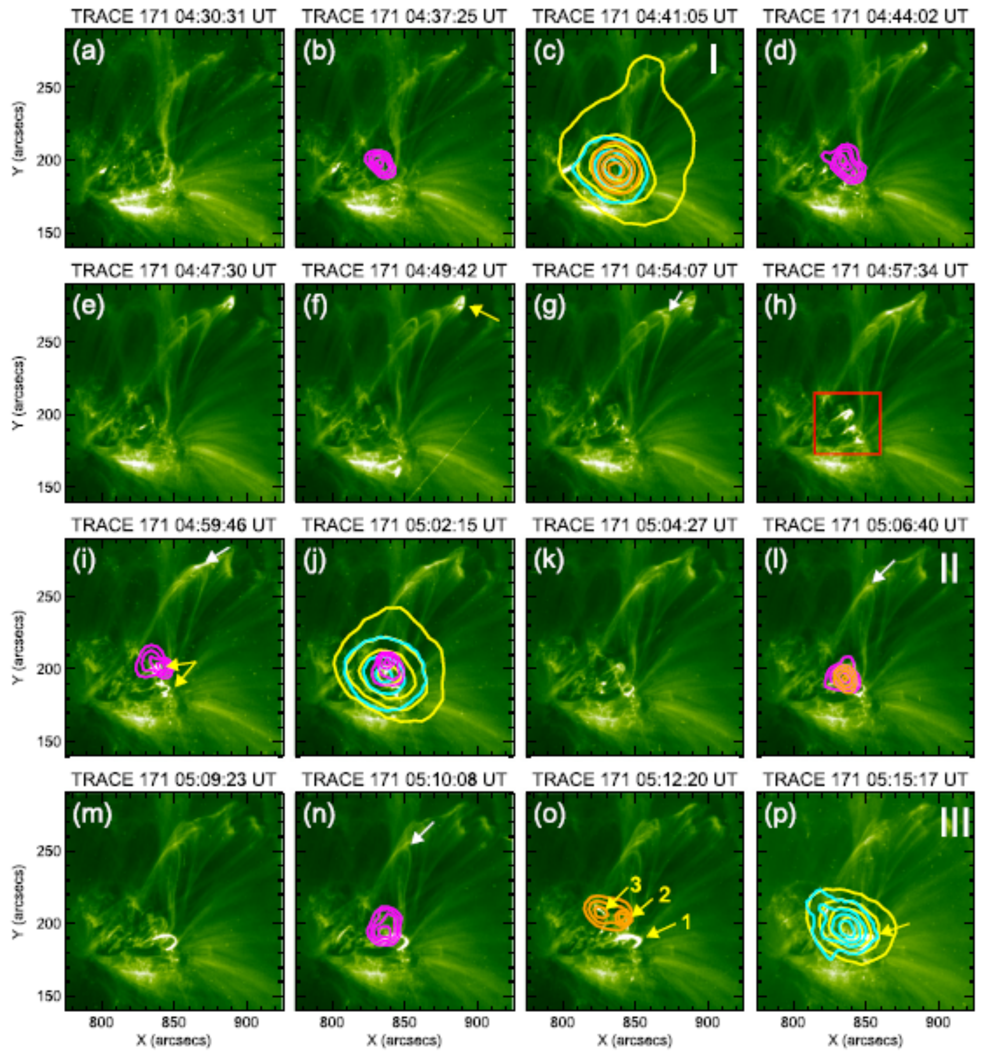

6-12 keV: magneta, 12-25 keV: orange, 17 GHz: yellow, 34 GHz: sky

- ❑ Overlying loop system was subjected to an altitude decrease of ~20Mm (40% of the initial height) for an extended span of ~30 minutes.
- ❑ Loop contraction is accompanied by HXR, MW and EUV brightening in the core region.

Converging motion of footpoint sources/ flare ribbons SOL2004-11-01 (M1.1)

Ji et al. 2006, ApJL

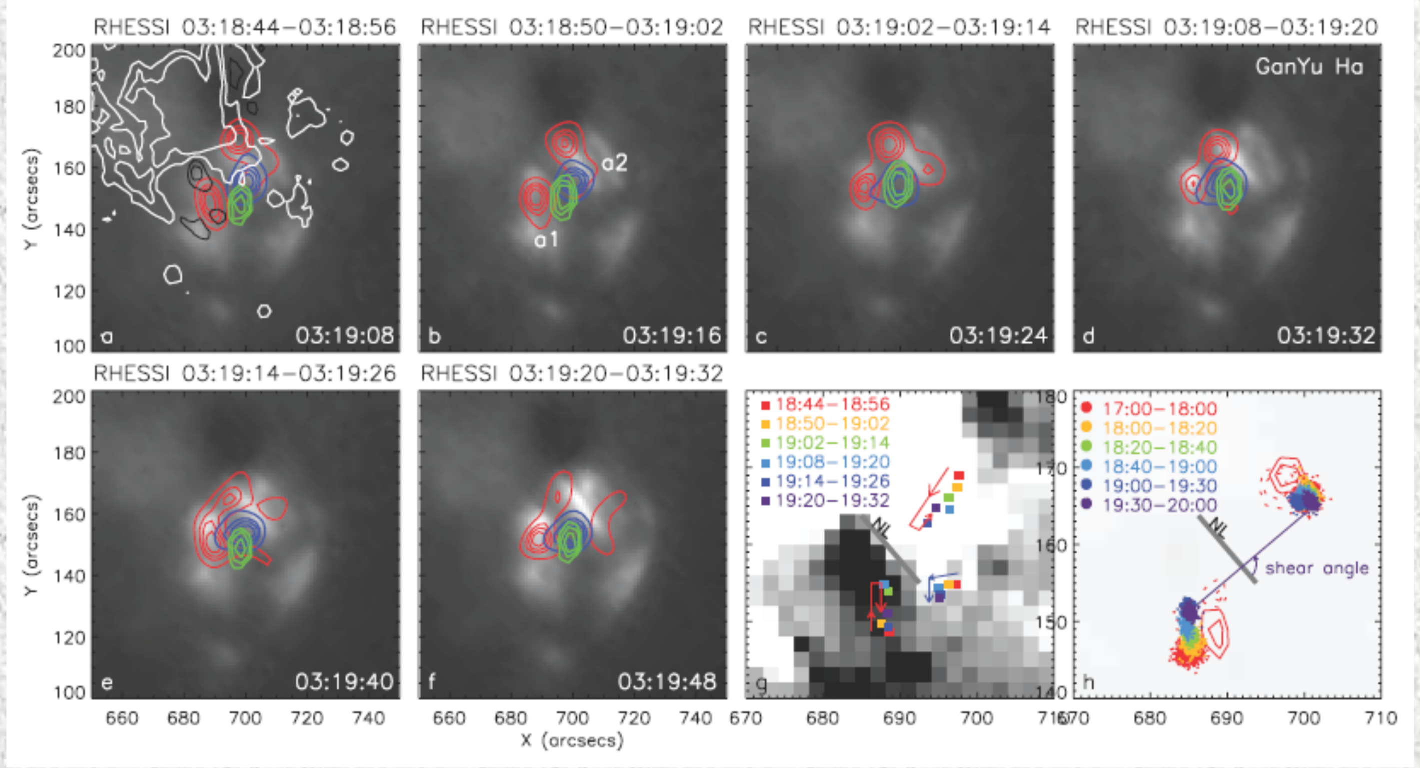

25-60 keV: red, 3-8 keV: blue, 17 GHz: green

- ❑ Converging motions are confirmed by both Hα and HXR measurements.
- ❑ Shear angle decreases during the converging motion showing the relaxation of a sheared magnetic field.

Unshearing motion of foot-point sources and LP source
SOL2003-10-29 (X10)
Liu, Petrosian, Dennis & Holman 2009

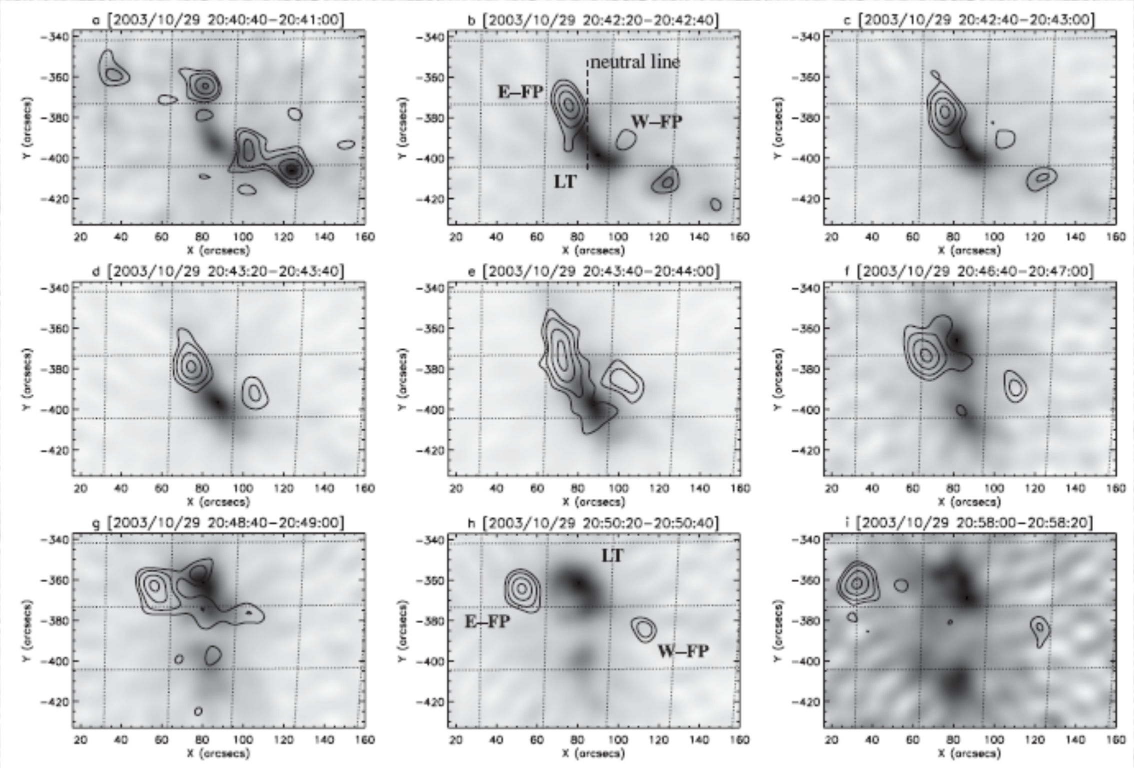

12-25 keV: gray scale; 60-100 keV: contours

- The double FPs first move toward and then away from each other, mainly parallel and perpendicular to magnetic neutral line, respectively.
- The transition of these two phases of FP unshearing motion coincides with the direction reversal of the motion of the LT source.

Converging motion of HXR sources during a sigmoid eruption SOL2013-04-11 (M6.5)

(Kushwaha, Joshi, et al. 2015, submitted)

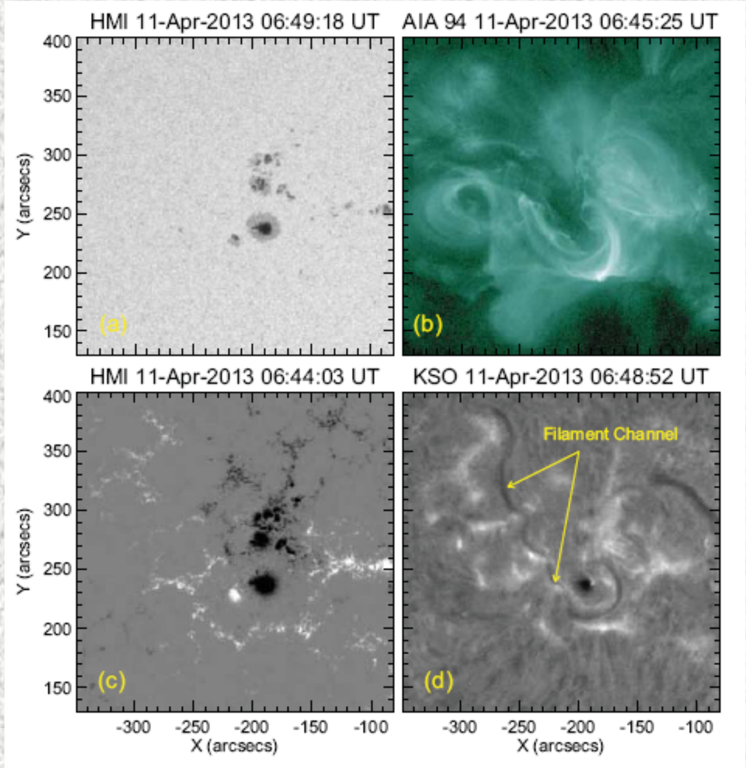

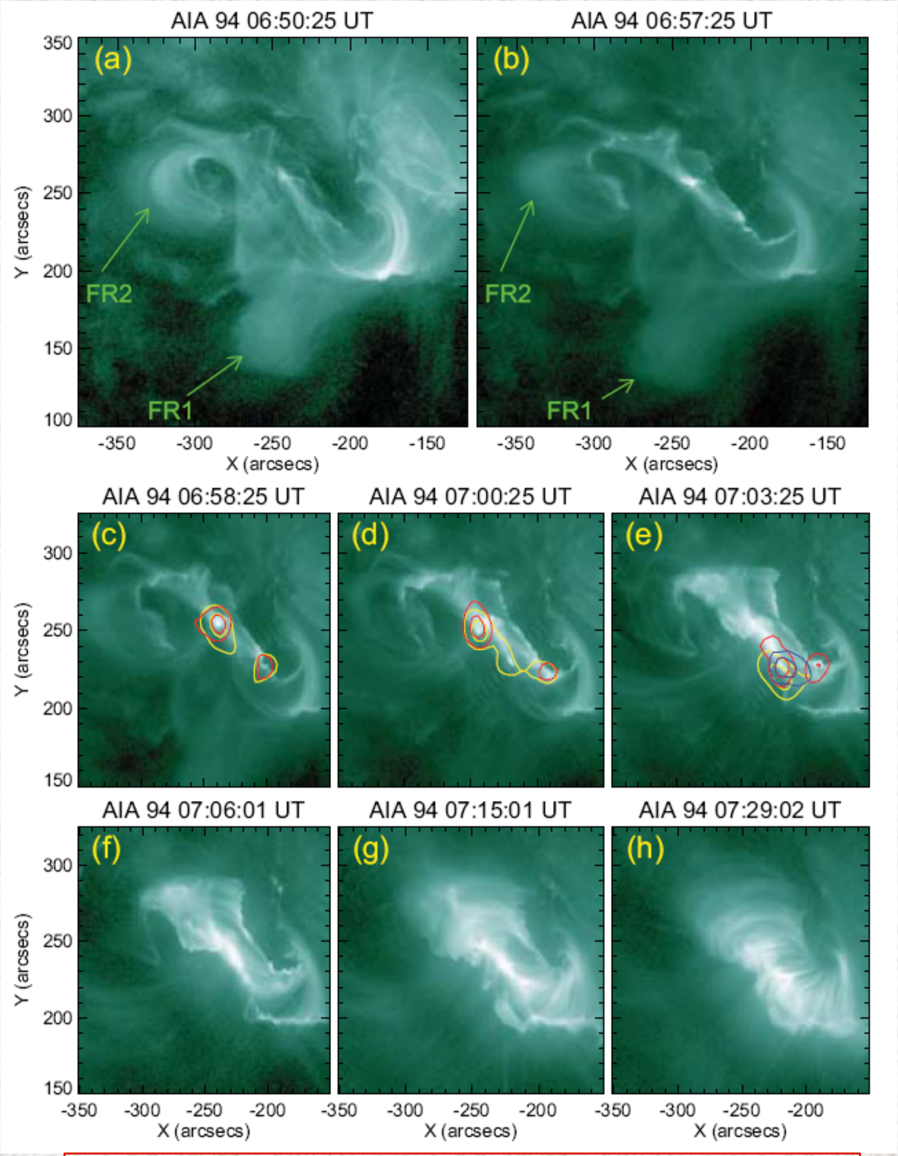

- Prolonged rise phase of ~21 minutes.
- FP HXR sources exhibit converging motions.

12-25 keV: yellow, 25-50 keV: red, 50-100 keV: blue

Converging motions: HXR sources and flare ribbons SOL2013-04-11 (M6.5)

(Kushwaha, Joshi, et al. 2015, submitted)

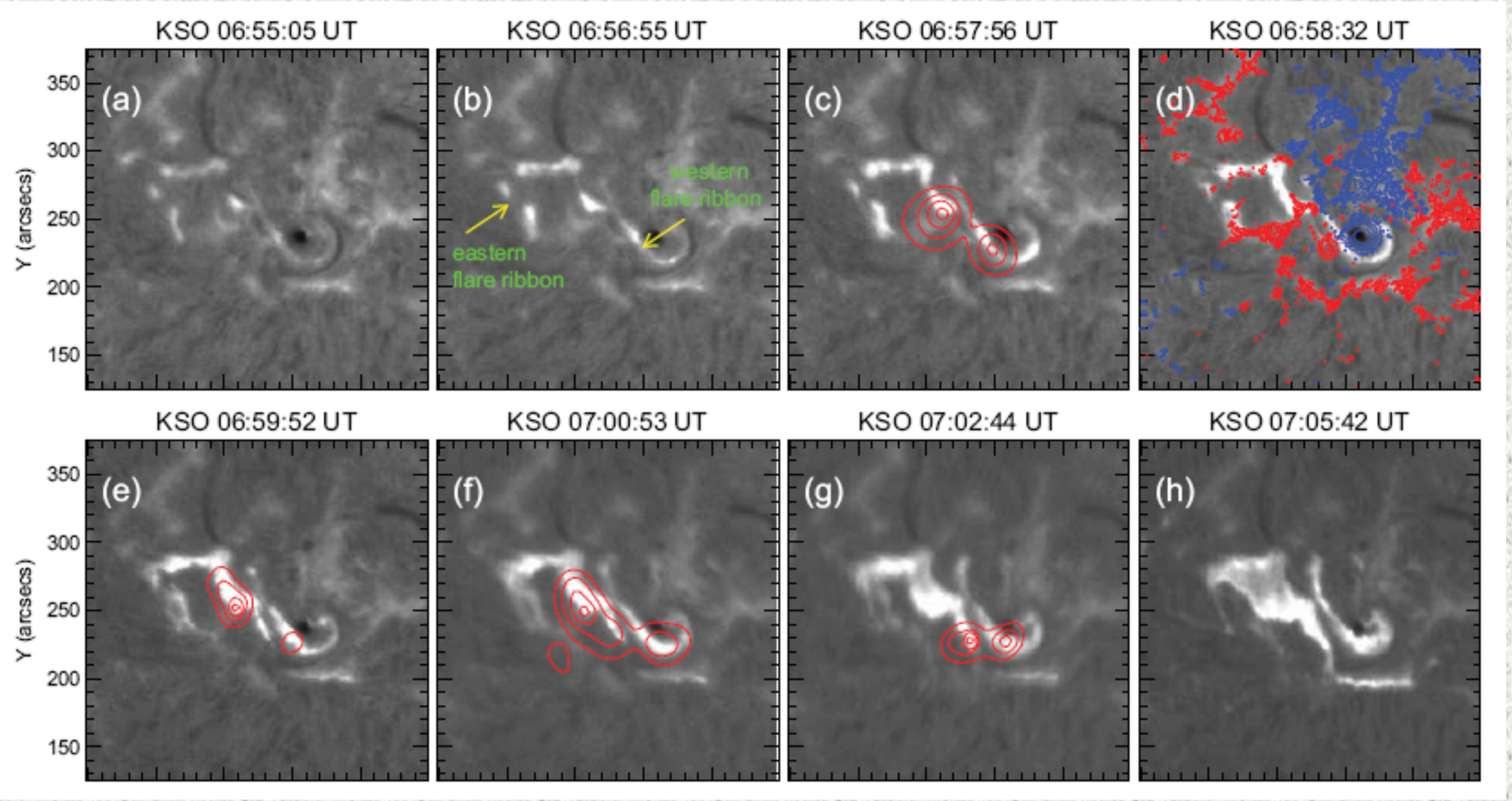

25-50 keV: red contours

- Ribbons/FPs move parallel to polarity neutral line.

HXR sigmoid during initial phase of SOL2003-11-20
Ji et al. 2008, ApJ

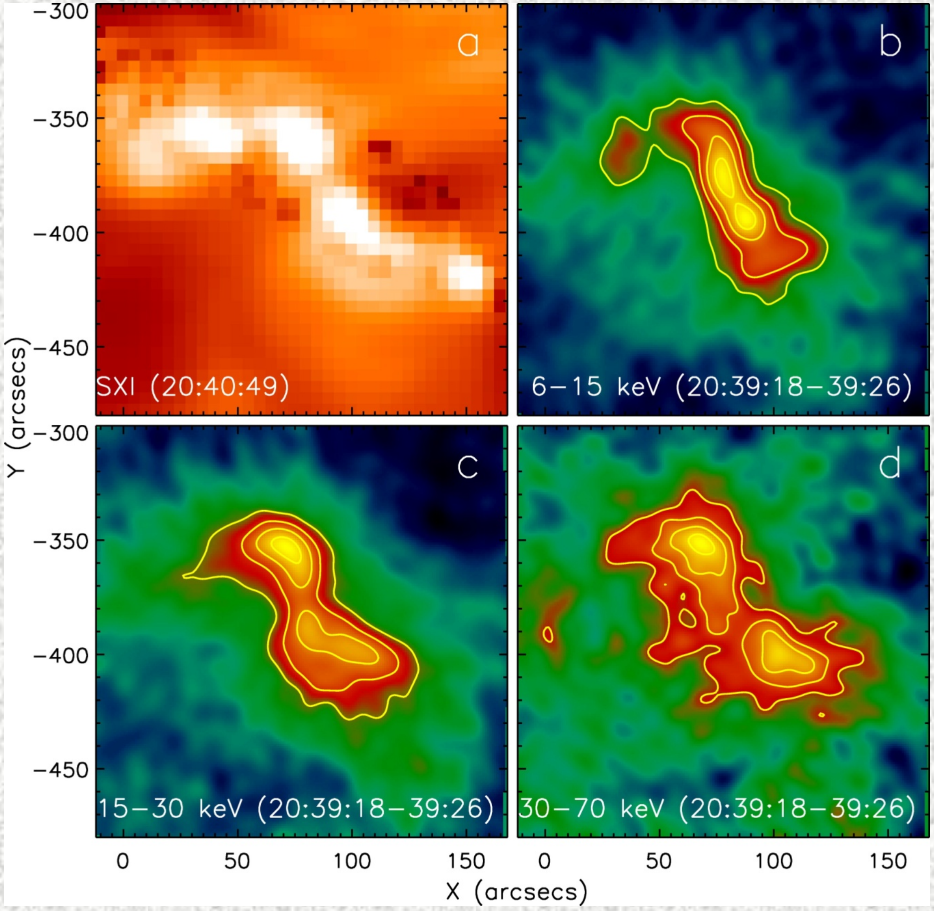

- ❑ HXR sigmoid structure during the initial phase of the flare.
- ❑ Soft X-ray counterpart of HXR sigmoid is seen in SXI images.

Rainbow reconnection model (Somov 1986, 2002)

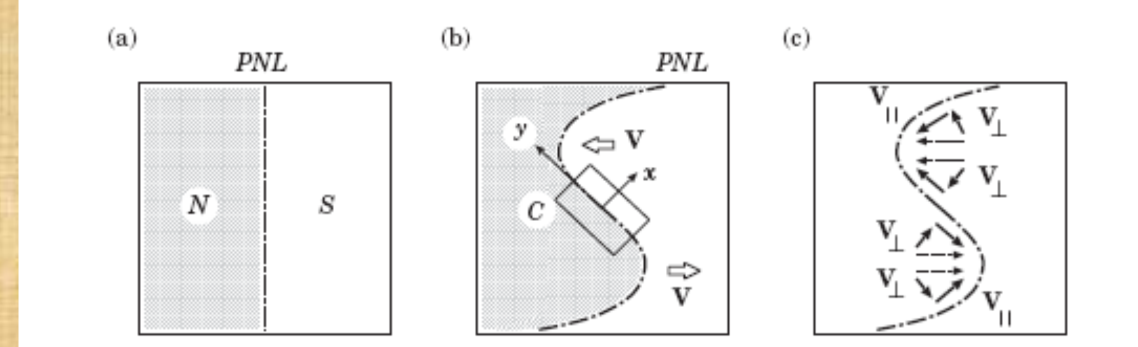

A large-scale vortex flow in the photosphere distorts the PNL

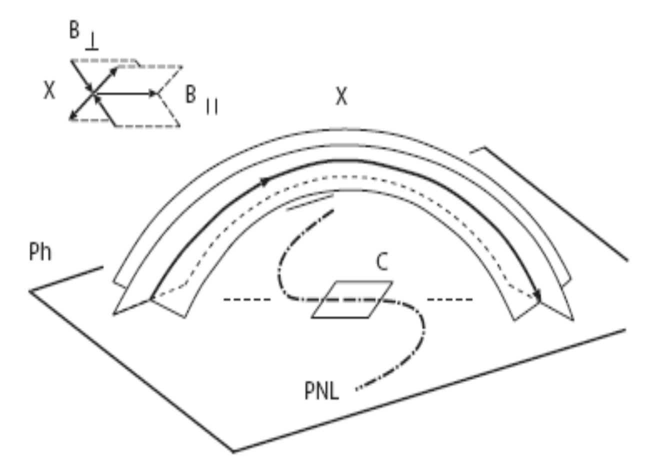

"Rainbow reconnection" model. Separator X above the S-shape d bend of PNL.

Before a large two ribbon flare, the bases of magnetic field lines are moved by two types of large scale photospheric flows:

(1) Converging flows: Directed to PNL, create the pre-flare current layers in the corona and provide an excess of magnetic energy sufficient to produce a flare.

(2) Shear flows: Parallel to PNL, increase the length of field lines in the corona and, therefore, produce an excess of energy too.

During a flare when the energy release takes place, the model describes two kinds of apparent motion for LT and FP sources.

Explanation of RHESSI observations of 'flare rise phase' in terms of rainbow reconnection model

Joshi et al. 2009, ApJ, 706, 1438-1450

See also RHESSI Science Nugget 120

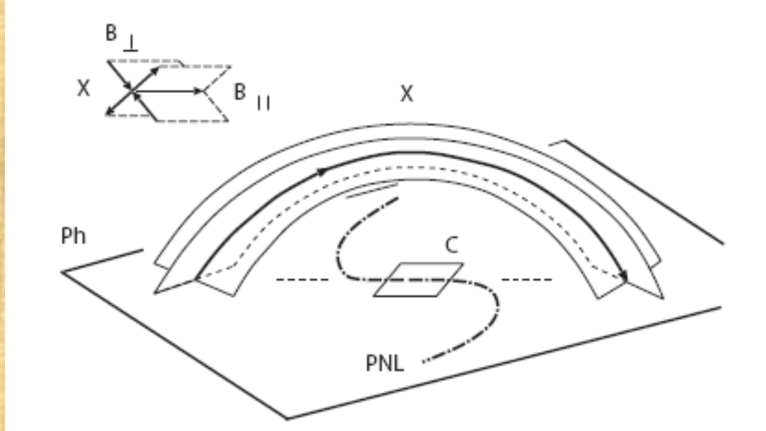

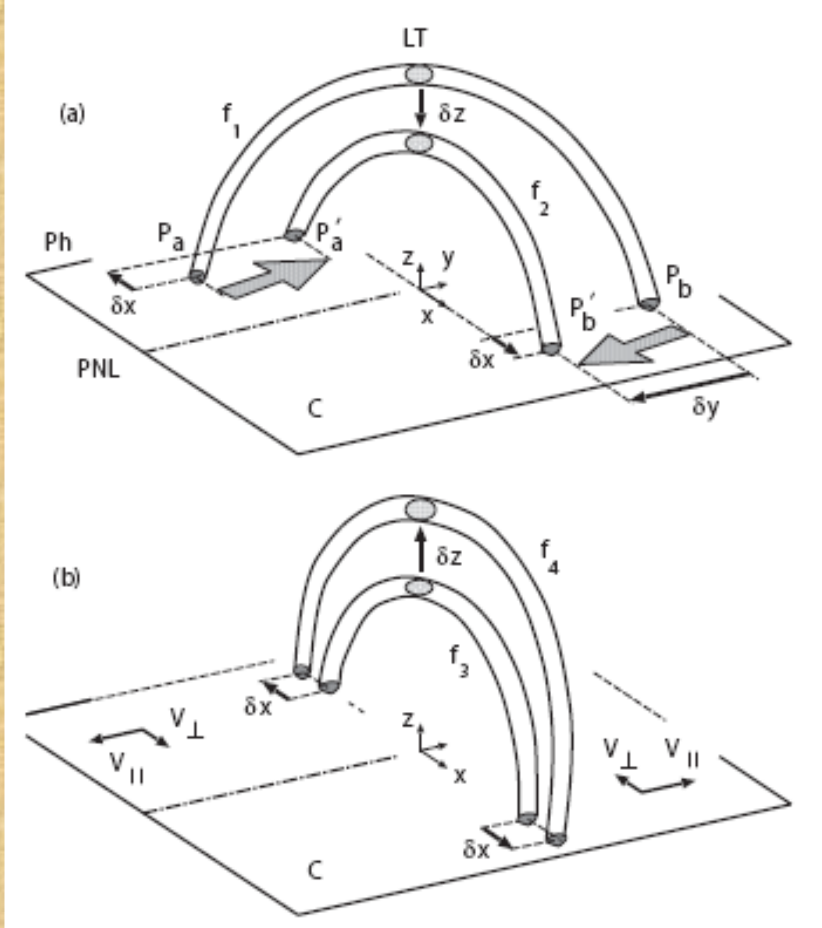

Interpretation of flare evolution in terms of the rainbow reconnection model (Somov 1986). **(a) First phase:** the main role o f reconnection is to release the excess of magnetic energy genera ted before a flare as result of photospheric s hear flows (LT altitude decrease and convergin g motion of FP sources).
(b) Second phase: reconnection involves magnetic field lines rooted successively ap art from the PNL.

Thermal and non-thermal energy SOL2004-07-14 (M6.2)

(Kushwaha, Joshi, et al. 2015, ApJ, 807, 101)

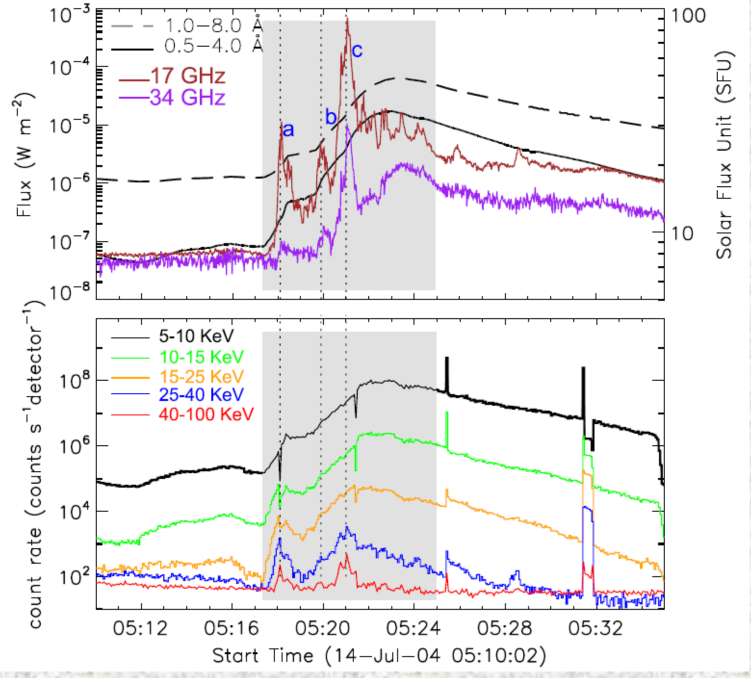

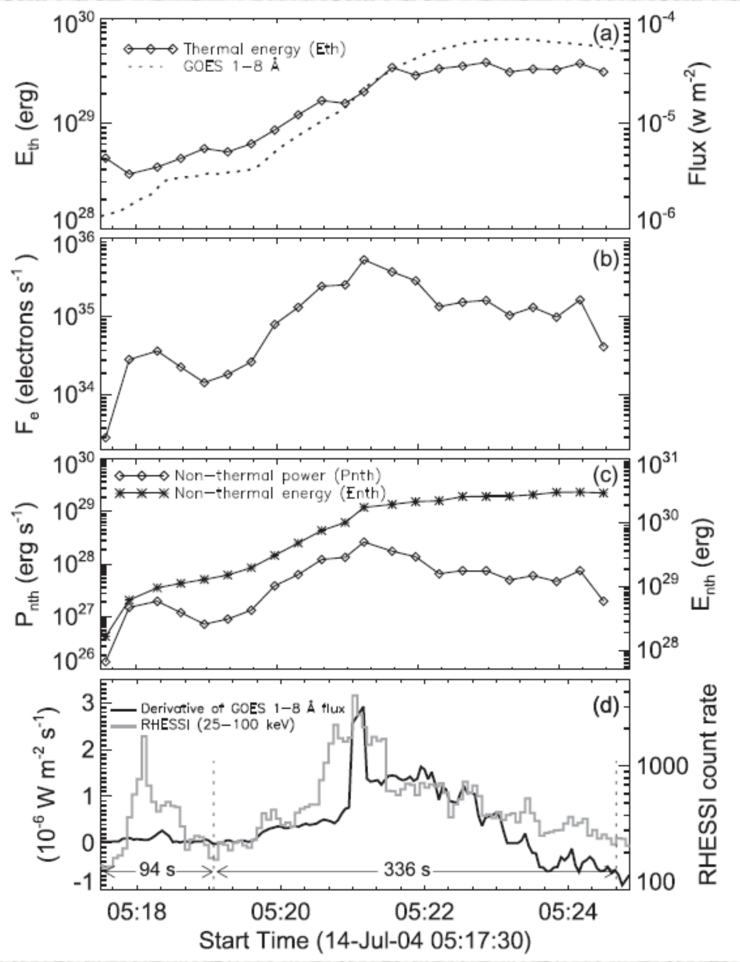

Flare characteristics	Parameters
Duration of HXR impulsive phase	430 s
No. of HXR peaks	2
	94 s and 336 s
Total non-thermal energy ($(E_{nth})_{tot}$)	3.03×10^{30} erg
Thermal energy (E_{th})	
-Thermal energy $(E_{th})_{max}$	3.89×10^{29} erg
-Thermal energy $(E_{th})_{min}$	0.33×10^{29} erg
$(E_{nth})_{tot}/(E_{th})_{max}$	~ 7.5

$$E_{th} = 3k_B T n V = 3k_B T\sqrt{EM \cdot f \cdot V}\ [\text{erg}]$$

$$P_{nth}(E > E_{LC}) = \frac{\delta - 1}{\delta - 2} F_e E_{LC} 10^{35} \left[\text{erg s}^{-1}\right]$$

HXR observations of a confined flare and associated magnetic transients

SOL2011-09-26 (M4.0)

Kushwaha, Joshi, et al. 2014, ApJ

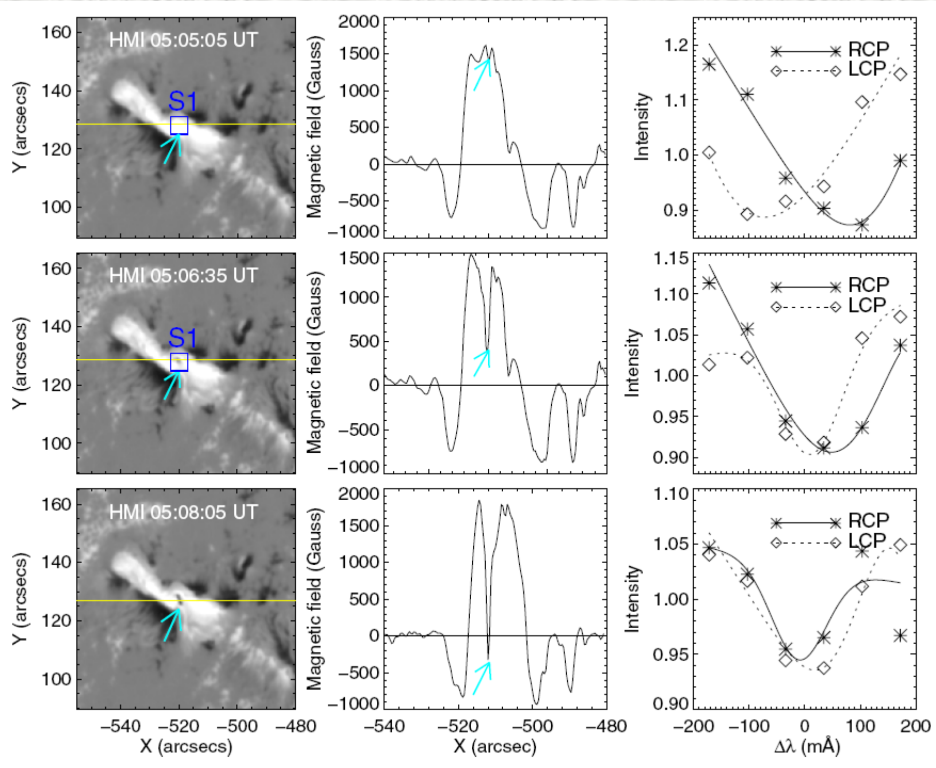

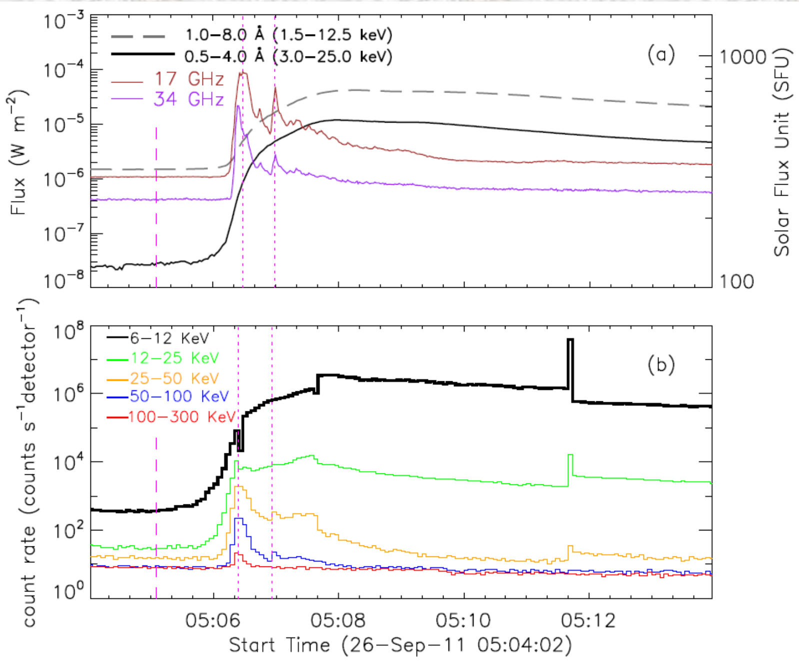

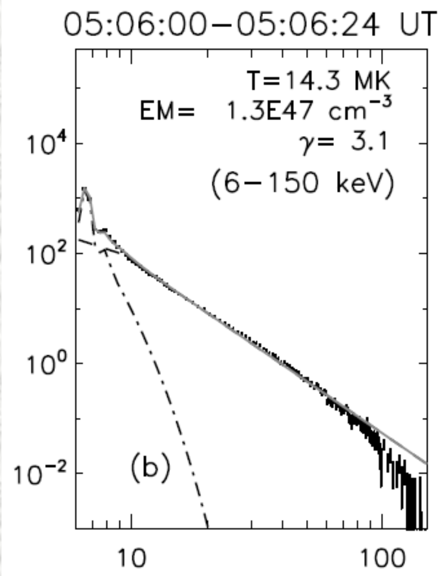

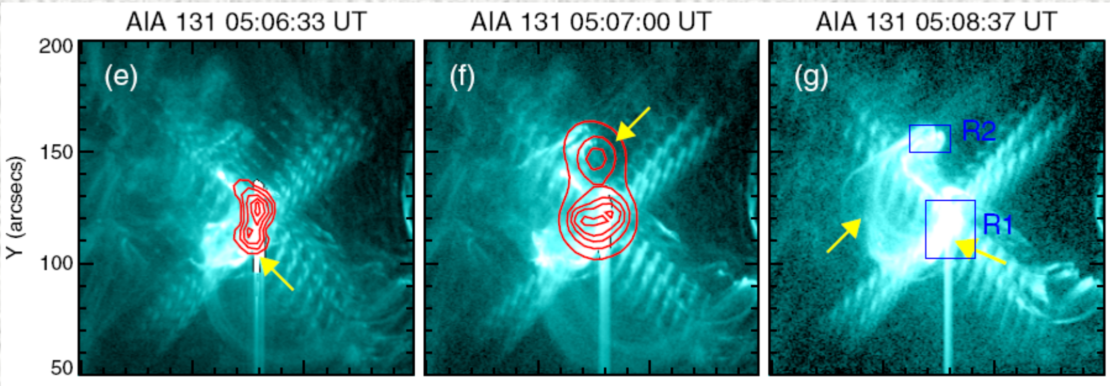

Precursor phase of solar flares

(Chifor et al. 2006, 2007; Joshi at al. 2011)

- ***SOL2003-11-01 (M3.2)***
  (Joshi at al. 2011, ApJ, 743, 195)
- Evidence of localized energy release and non-thermal emission in the precursor phase.

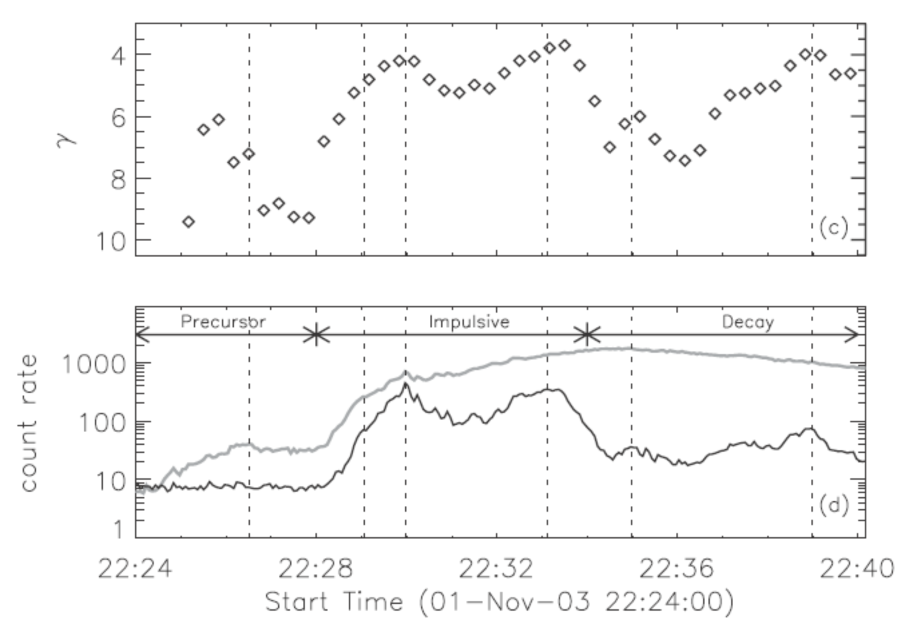

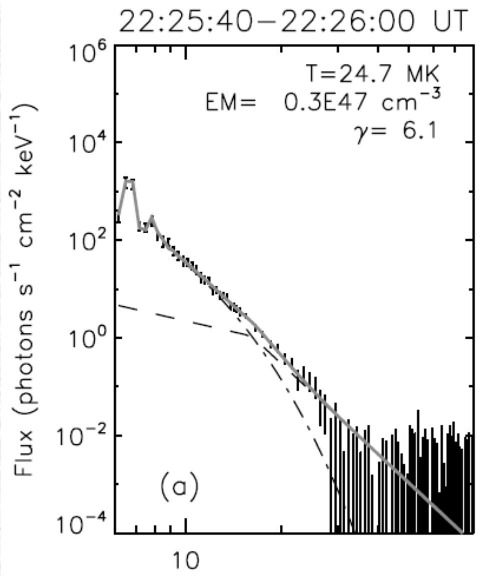

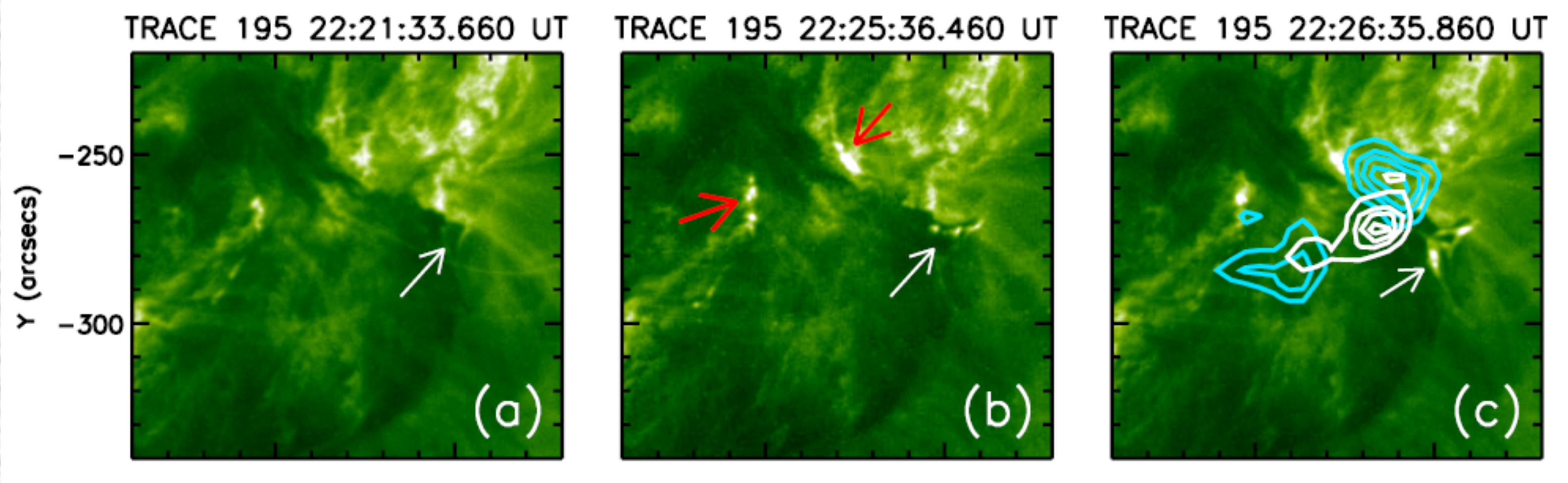

6-12 keV: blue
12-25 keV: white

HXR coronal emission associated with kink instability

SOL2004-08-18 (X1.8)

(Joshi et al. 2013, ApJ; Cho et al. 2009, ApJ)

50-100 keV: blue contours

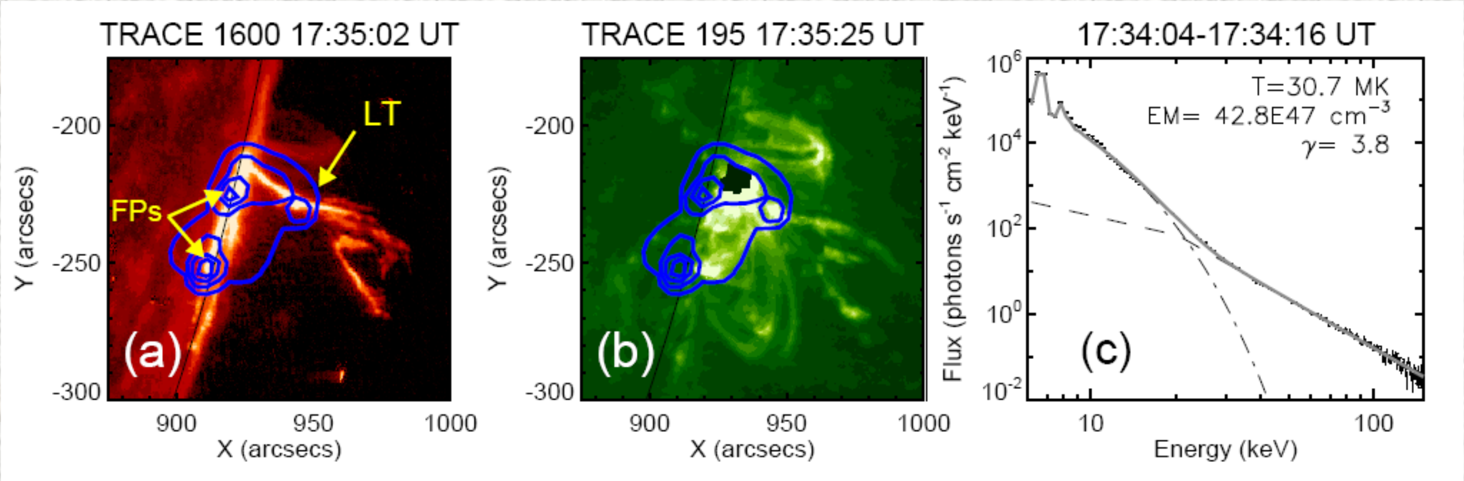

SOL2002-05-27 (M2)

(Alexander et al. 2006, ApJ; Ji et al. 2003 ApJ)

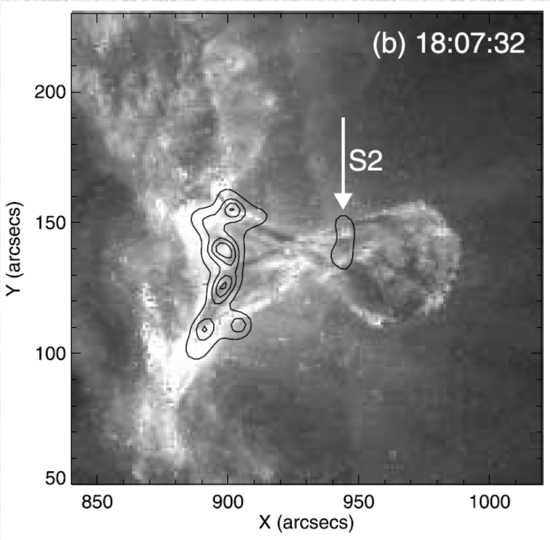

SUMMARY

- ❑ RHESSI has given us a systematic view of X-ray coronal sources that combines high spatial and spectral resolution with broad energy coverage and high sensitivity.

- ❑ Despite the low density and hence bremsstrahlung efficiency of corona, we now detect coronal hard X-ray emission from sources in all phases of solar flares. They are believed to occur closest to the electron acceleration site.

✓ Strong non-thermal source in corona
✓ Large-scale contraction of loops in the early phase
✓ Double coronal sources

- ❑ Understanding of X-ray precursor phase.

- ❑ Unshearing motion of foot-point sources.

- ❑ Observations of early rise phase are very important as they show deviation from the standard flare model.

THANKS